

RAMAN Scattering

Rico Schmidt and Guido Falk von Rudorff (Group M4)

I Introduction

The focus of this experiment is to observe inelastic scattering of a photon, namely the RAMAN process. The scattering targets are solids throughout the whole experiment. RAMAN scattering is useful in order to analyze a given sample for the contained elements and the molecular structure as both properties heavily influence the RAMAN spectrum.¹

I.A Raman Scattering

As RAMAN scattering is an inelastic process, the energy of the incident photon and the energy of the emitted one are different. Hence, the total process is a two photon process.² In general, there is no constraint forcing the energy difference to have a specific sign, as the energy transfer is caused by phonons. If the energy of the incident light is higher than the one of the emitted light, a phonon carrying the energy difference is created, whereas an inverted energy relation requires the annihilation of a photon in order to add the required energy to the scattered photon. The former case gives the STOKES component, whereas the latter case leads to the anti-STOKES component in the spectrum.²

The two STOKES components depicted in Figure 1 can be derived by expanding the polarizability \mathbf{p} as TAYLOR series in a phonon mode μ . For simplicity, we will assume the polarizability to be a scalar p .

$$p = \sum_{i=0}^{\infty} \alpha_i \mu^i \simeq \alpha_0 + \alpha_1 \mu + \alpha_2 \mu^2 \quad (1)$$

where μ is a photon of frequency Ω

$$\mu = \mu_0 \cos \Omega t \quad (2)$$

Now we can analyze the response of the material in an external field

$$E = E_0 \cos \omega t \quad (3)$$

In the order 0, we see no interaction, as p is independent from μ . The resulting radiation is the elastic RAYLEIGH scattering: the energy of the photon is conserved. In the first order approximation, we get

$$\begin{aligned} Ep &= \alpha_0 E + \alpha_1 \mu E \\ &= \alpha_0 E + \alpha_1 \mu_0 \cos(\Omega t) E_0 \cos(\omega t) \end{aligned} \quad (4)$$

Using the geometric identity

$$\cos\left(\frac{a+b}{2}\right) \cos\left(\frac{a-b}{2}\right) = \frac{1}{2}(\cos a + \cos b) \quad (5)$$

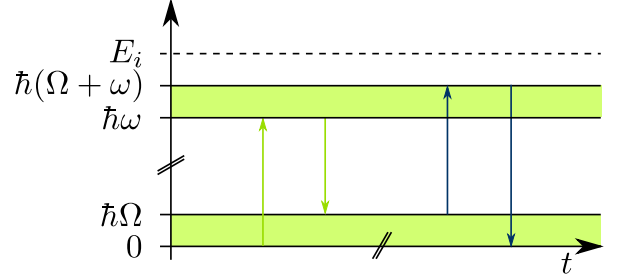


Figure 1. Energy levels⁵ for the STOKES component (left, green arrows) and the anti-STOKES component (right, blue arrows) for a single phonon of frequency Ω and incident radiation with frequency ω . In case one of the energy levels above the discontinuity would match an energy level E_i of an electron, the process is called *resonant* RAMAN scattering.

with $a = (\omega + \Omega)t$ and $a = (\omega - \Omega)t$, we get a first order response of

$$\frac{\partial(Ep)}{\partial\alpha_1} = \frac{1}{2} \mu_0 E_0 \left[\underbrace{\cos((\omega - \Omega)t)}_{\text{STOKES}} + \underbrace{\cos((\omega + \Omega)t)}_{\text{anti-STOKES}} \right] \quad (6)$$

Usually, the photon energy is about 100 times higher than the phonon energy.³ The first order RAMAN effect can be seen as an absorption process.⁴

Of course, this method can be repeated in order to derive the second order approximation which involves two phonons

$$\begin{aligned} \frac{\partial(Ep)}{\partial\alpha_2} &= \mu_0^2 E_0 \cos^2(\Omega t) \cos(\omega t) \\ &= \frac{\mu_0^2 E_0}{2} [\cos((\omega - \Omega)t) + \cos((\omega + \Omega)t)] \cos(\Omega t) \\ &= \frac{\mu_0^2 E_0}{4} [\cos((\omega - \Omega - \Omega)t) + \cos((\omega - \Omega + \Omega)t) + \\ &\quad \cos((\omega + \Omega - \Omega)t) + \cos((\omega + \Omega + \Omega)t)] \\ &= \frac{\mu_0^2 E_0}{4} [\cos((\omega - 2\Omega)t) + \cos((\omega + 2\Omega)t) + \\ &\quad 2 \cos(\omega t)] \end{aligned} \quad (7)$$

The two photon process contributes to the RAYLEIGH component with half of the total intensity of the second order. In this case, either a phonon is first created and then annihilated or the other way round. As the probability of the order generally depends on the occupation number of the photon mode Ω , for most system temperatures, the former ordering is the more common one. As even the first order term is very small, second order approximation is far less likely to be observed.² For this derivation of the second order scattering, we assumed

the two phonons to have the same energy as they share a common frequency Ω . This restriction does not hold for real events, which may involve different energies and, hence, create highly complicated spectral lines.² In that case, only the sum of the \mathbf{k} vectors of the phonons have to be small. Hence, much more states may contribute to the RAMAN signal.⁶

This classical approach is suitable to explain the RAMAN shift, that is the energy difference of the RAYLEIGH and STOKES components. However, it is impossible to explain the relative intensities without quantum mechanical methods.⁷ For small phonon energies, the displacement potential can be approximated as harmonic oscillator.⁷ This approximation gives a regular lattice, which can be treated with internal lattice coordinates.² As RAMAN scattering is restricted to optical phonons,^{2,3} the lattice coordinates only have to describe displacements which do not result in synchronous oscillations of the whole lattice, which they are perfectly capable of. Despite the lengthy prefactors,⁷ the overall dependency for the intensities is²

$$I(\omega \pm \Omega) \propto |\langle n \mp 1 | \hat{\mu} | n \rangle|^2 \quad (8)$$

where n is the number of phonons in the mode of frequency Ω . As $\hat{\mu}$ is the interaction operator for the RAMAN process, it can be written—disregarding prefactors—as a sum of the creation operator \hat{a}^\dagger and the annihilation operator \hat{a} . Together with the definition of these operators for a harmonic oscillator, we get

$$I(\omega \circ \Omega) \propto n + \delta_{\circ-} \quad \circ \in \{+, -\} \quad (9)$$

This relation between the intensities and the occupation number is the key in order to understand the influence of the temperature. For phonons, the occupation numbers is given by the BOLTZMANN distribution

$$n \propto \exp\left(-\frac{E_n}{kT}\right) = \exp\left(-\frac{\hbar\Omega(n+1/2)}{kT}\right) \quad (10)$$

For the relative intensities, we can make use of both proportionalities

$$\begin{aligned} \frac{I(\omega - \Omega)}{I(\omega + \Omega)} &= \frac{n+1}{n} \\ &= \frac{\exp\left(-\frac{\hbar\Omega(n+3/2)}{kT}\right)}{\exp\left(-\frac{\hbar\Omega(n+1/2)}{kT}\right)} \\ &= \exp\left(\frac{\hbar\Omega}{kT} \left(n + \frac{3}{2} - n - \frac{1}{2}\right)\right) \\ &= \exp\left(\frac{\hbar\Omega}{kT}\right) \end{aligned} \quad (11)$$

For high temperatures, the quotient is one as there are enough phonons in order to equalize the probability of annihilation and creation. For low temperatures, the STOKES component is dominant. For two phonon RAMAN scattering, the relative intensities are the same.¹

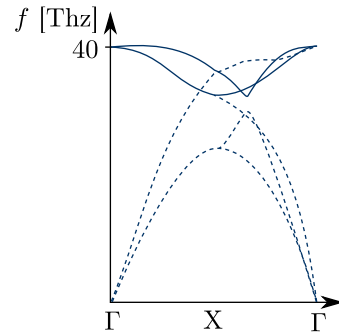


Figure 2. Phonon dispersion for diamond.⁸ Both optical (stroked) and acoustical (dashed) phonons are given. Theoretical values.

Over a broad range of temperatures, the STOKES components are shifted towards lower frequencies. This shift and the linewidth Γ in the spectrum depend on the spectrum in a mostly non-analytical fashion.¹

It has to be noted, however, that the intensities of both the STOKES and the anti-STOKES component are very small compared to the elastic RAYLEIGH scattering.²

The total scattering probability can be derived⁸ using FERMI's Golden Rule and reads^{8,9}

$$P \simeq \frac{2\pi}{\hbar} \left| \frac{\langle 0 | H_{e-r} | a \rangle \langle a | H_i | b \rangle \langle b | H_{e-r} | 0 \rangle}{(\hbar\omega_i - E_a + i\Gamma)(\hbar\omega_s - E_b + i\Gamma)} \right|^2 \quad (12)$$

where H_{e-r} is the coupling Hamiltonian between photon and electron, H_i is the interaction Hamiltonian between the intermediate states $|a\rangle$ and $|b\rangle$ which can be both real or virtual states. In the former case, the process is called resonant RAMAN scattering and is of much higher intensity¹ than the normal RAMAN scattering process.

I.B Experimental Setup

The shifts for the samples used in this experiment are listed in Table I. Figure 2 shows the dispersion relation for diamond. For the center of the BRILLOUIN zone, Γ , the frequency of the optical phonons matches the RAMAN shift in Table I.

Table I. Reference¹ lines for RAMAN scattering.

material	RAMAN shift [cm ⁻¹]
Diamond	1332.5
Graphite	1575.0 (strong) 1355.0 (weak)
Si	520.2
CaF ₂	332.0

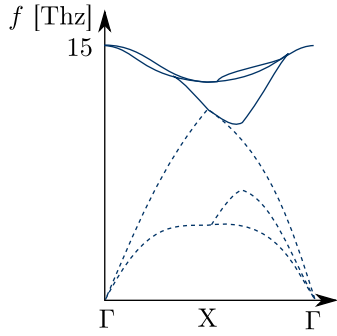


Figure 3. Phonon dispersion for silicon.⁸ Both optical (stroked) and acoustical (dashed) phonons are given. Theoretical values.

I.C Preliminary Calculations

The energy of a phonon is given by

$$E = hf = \frac{hc}{\lambda} = hc\tilde{\nu} \quad (13)$$

For the Si(111) peak at 521 cm^{-1} , the phonon energy is about 64.6 meV. This is comparable to the thermal energy at room temperature which is given by

$$E = kT \quad (14)$$

and evaluates to some 25 meV. According to eqn. 11, this gives relative intensities of

$$\frac{I(\omega - \Omega)}{I(\omega + \Omega)} \simeq 13.2 \quad (15)$$

Hence, the STOKES component is expected to be of much higher intensity than the anti-STOKES one. For lower temperatures, this effect is expected to get more important, whereas for higher temperatures, the relative intensity should approach one. Due to the high-intensity laser radiation, the sample is expected to heat up significantly.

For the laser radiation of 532 nm, the wavenumber is given by

$$\nu = \frac{2\pi}{\lambda} \simeq 1.2 \cdot 10^5 \text{ cm}^{-1} \quad (16)$$

and the single photon momentum evaluates to

$$p = \hbar k \simeq 1.25 \cdot 10^{-27} \text{ Ns} \quad (17)$$

Table II. Position of the STOKES and anti-STOKES component 532 nm laser radiation.

material	anti-STOKES [nm]	STOKES [nm]
Diamond	497.0	572.3
Graphite	490.9	580.7
	496.2	573.3
Si	517.7	547.1
CaF ₂	522.8	541.6

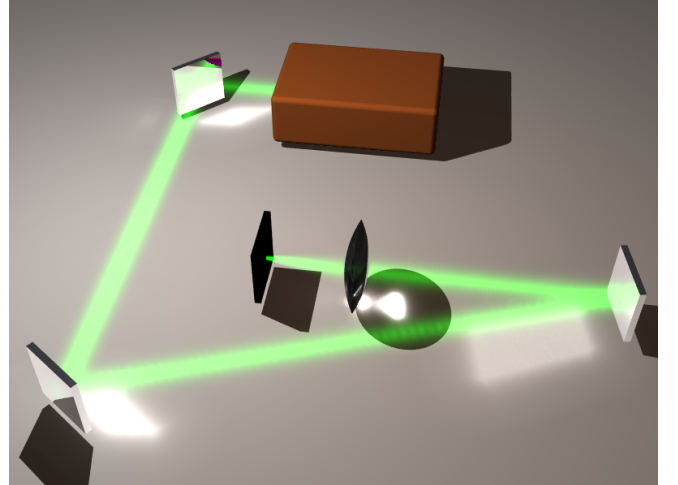


Figure 4. Experimental setup with the laser (brown) and target (black). The fiber to the spectrometer was placed behind the rightmost mirror. The height difference between laser and sample is not shown in this figure. All mirrors can be tilted, the sample mount has two degrees of freedom.

The size of the BRILLOUIN zone d is the inverse of the lattice constant $a = 0.543 \text{ nm}$. With $d = 1.84 \text{ cm}^{-1}$, the BRILLOUIN zone is much larger than the photon wavenumber. Therefore, we expect⁸ the occurrence of phonons with small k due to conservation of momentum—see Figure 3.

Using the data from Table I, the expected wavelengths λ' for the STOKES and anti-STOKES component for Nd:YAG laser light at $\lambda = 532 \text{ nm}$ can be calculated.

$$\lambda' = \frac{2\pi}{\frac{2\pi}{\lambda} + \tilde{\nu}} \quad (18)$$

The results are given in Table II.

II Experimental Setup

Figure 4 illustrates the experimental setup. A 200 mW Nd:YAG laser emits frequency doubled light at 532 nm. The first and second mirror are necessary in order to cope with the height difference between the laser and the sample. In general, they would be optional. Actually, the last mirror is a notch filter that diminishes the initial laser light at 532 nm. For other wavelengths, this filter is nearly transparent, so both the STOKES and anti-STOKES component can pass through this filter right into the entry lens of a fiber connected to the grating spectrometer. However, the beam profile may get altered by the notch filter as shown in Figure 5.

All the samples are put on the sample holder by using the adhesive forces of a single drop of water between the sample and the sample holder. First, we mounted the diamond sample which is said to have a high-intensity RAMAN components and aligned the mirrors in order to assure the sample to be in the focal point of the objective.

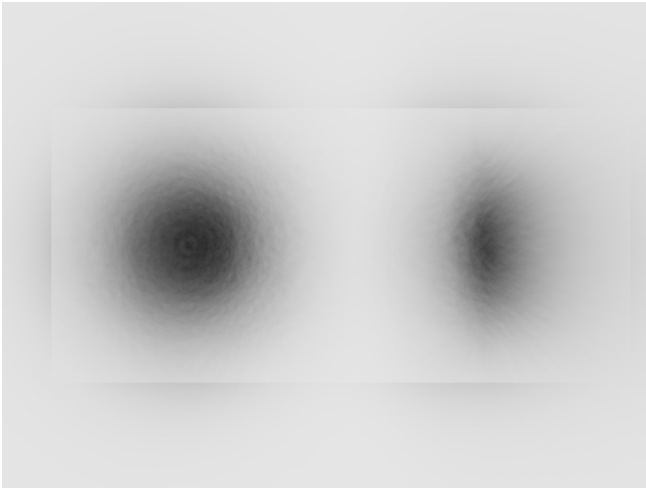


Figure 5. Influence of the notch filter on the RAMAN components (simulation using raytracing, inverted). The left beam has a natural gaussian profile after passing a glass pane perpendicular to the wave vector. The right one shows had a gaussian beam profile before passing a thick glass pane that has been tilted by 45 degrees. In case the beam radius is comparable to the glass pane, the beam profile is highly distorted. The light squares represent the size of the square glass panes.

This required several rounds of optimization, as tilting one of the first mirrors leads to a very different beam direction near the sample. The most difficult yet crucial part was centering the laser beam within the objective. This is a mandatory requirement of the setup, as the RAMAN components have to be collected by the objective as well. Even after a very careful adjustment, we were unable to obtain any signal despite the 532 nm peak.

The high efficiency of the notch filter could be easily observed by placing a paper as reflection screen right behind the filter. However, we tried to suppress the impact of the direct incident beam on the intensity measured by the spectrometer even more. Therefore, we increased the angle between the incident and the reflected beam at the notch filter by both moving the notch filter closer to the sample and moving the second mirror closer to the notch filter. On one hand, this setup is more difficult to adjust as most of the knobs are quite near to any of the beams. On the other hand, the entry lens of the fiber is only illuminated by light reflected back from the sample. Of course, this light is still dominated by RAYLEIGH scattering.

All spectra a recorded by averaging the spectrometer signal over a duration of 1-5 s. The background noise has been filtered out by recording a dark frame and subtracting this dark frame from the measured spectra. In order to cope with the stray light, we turned off the lights for the measurements and blacked out the windows. Strictly speaking, the dark frame should handle that influence, so this was optional for the measurements.

III Measurements

III.A Diamond

Optimizing the existing setup did not lead to any visible peaks in the spectrum despite the RAYLEIGH scattering. So we changed the setup as described in the previous paragraph and restarted the calibration. Figure 6 shows the first spectrum that contained a RAMAN component that is distinguishable from the background noise. The spectrometer often showed a rather strange behaviour: if we unscrewed the fiber from the spectrometer and looked at its end, we could see yellow or orange light—as expected for the STOKES component for the diamond sample. However, even if this yellow light was visible to the naked eye, the spectrometer did not measure any peak despite the RAYLEIGH one. In order to find an explanation for this measurement results, we pointed the fiber entry lens towards the green control LED from the spectrometer and got no signal. However, the light of the control LED of the computer screen gave an visible signal when analyzed by the spectrometer. As the latter LED was much brighter than the former one, we concluded that the threshold intensity, that is the minimal detectable intensity, is rather high for this spectrometer. As the RAMAN components are very weak, this explains the problems with recording other spectra which will be subject to further discussion.

Having a measureable signal, we put a piece of paper in the gap between notch filter and fiber entry lens. By looking at this paper using the security glasses that suppress the RAYLEIGH component at 532 nm just like the notch filter does, we were able to observe the inelastic scattered light. Although the objective should focus the light at one point, we always saw a filled circle on the paper. This may partially come from the notch filter, as shown in Figure 5. However, adjusting the objective and both the sample position and the incident mirror positions, we improved the signal to noise ratio and decreased the diameter of the filled circle described above. The blue line in Figure 6 represents the optimal spectrum we were able to record. In this spectrum, the STOKES component has about 44% of the intensity of the RAYLEIGH peak. Of course, due to the notch filter, this does not reflect the actual intensities of the light components that have been scattered back from the sample. The two spectra compared in Figure 6 are averaged over two different acquisition periods (see description). This has been necessary, as for the blue line, the spectrometer showed saturation effects (splitting of the RAYLEIGH component) already.

For both spectra, the STOKES component was detected at (572.75 ± 0.5) nm and the RAYLEIGH peak was found to be at (532.25 ± 0.5) nm.

III.B Other materials

Despite the extensive adjustment and optimization process, we were unable to record any spectrum for other

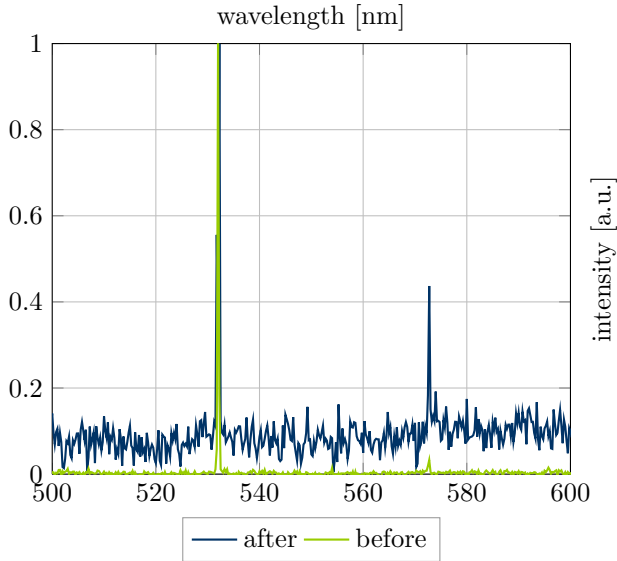


Figure 6. Measured spectra for the diamond sample before and after the second adjustment process. Both spectra have been scaled to set the intensity of the RAYLEIGH to 1. For both cases, the STOKES peak has been observed at 572.75 nm. The green line was the first spectrum with a distinguishable RAMAN component, the blue line shows the optimal signal we got after further optimization of the position of the objective. The different signal offset and noise level is caused by a different averaging time (1 s for the blue line, 5 s for the green one).

material. Cleaning the samples did not help either. In order to perform the remaining calculations, we analyzed old data from Group M6 which has performed the experiment on May 21st, 2012. The spectra have been averaged over 60 s each. Figure 7 shows the spectrum for silicon. As the anti-STOKES peak is very small, RAYLEIGH peak is not shown in its full height.

Given this data, the STOKES component for silicon was detected at (547.25 ± 0.5) nm and the anti-STOKES peak was found to be at (517.75 ± 0.5) nm. As the RAYLEIGH peak is saturated, the error estimate for the peak position is larger: (532 ± 1) nm. From the data in Figure 7, we got the peak positions for calcium fluoride. The anti-STOKES peak is at (523.0 ± 0.5) nm and the STOKES peak is at (541.25 ± 0.5) nm. As far as the last sample, graphite, is concerned, Table II makes clear that both the anti-STOKES components are out of the range of the spectrometer. However, the STOKES component could be detected at (580.0 ± 0.5) nm. For all these three measurements with foreign data, the position of the RAYLEIGH peak is the same as mentioned above.

For all the peaks, the RAMAN shift and the phonon energy is given in Tab III. The shift is determined by evaluating

$$\nu = \left(\frac{1}{\lambda'} - \frac{1}{\lambda} \right) \quad (19)$$

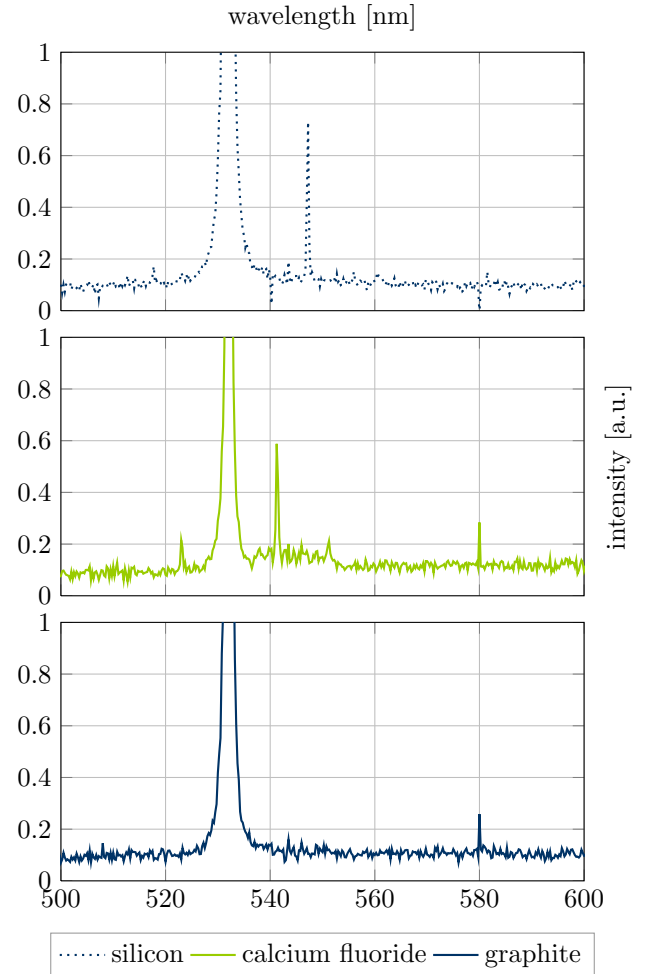


Figure 7. Measured spectra for the three other sample averaged over 60 s each. The Rayleigh peak is cut off in order to show the anti-STOKES component. In this arbitrary unit scaling and disregarding saturation effects, it would be around 7.6 for all spectra. For the peak positions, see text. (Measurement by Group M6, May 2012).

with the GAUSSIAN error estimate

$$\Delta\nu = \sqrt{\left(\frac{\partial\nu}{\Delta\lambda'} \right)^2 (\Delta\lambda')^2 + \left(\frac{\partial\nu}{\Delta\lambda} \right)^2 (\Delta\lambda)^2} \quad (20)$$

III.C Intensities

According to Table IV, the STOKES component is about 5-7 orders of magnitude smaller than the RAYLEIGH component. This motivates again the use of a notch filter. From the ratio for the STOKES and anti-STOKES peaks in Table IV together with the phonon energies in Table III, we can calculate the sample temperature from eqn. 11

$$T = \frac{\hbar\Omega}{k \ln(I_s/I_{as})} \quad (21)$$

Table III. Measured RAMAN shifts [cm^{-1}] and phonon energies [meV] for STOKES (s) and anti-STOKES (as) components. Reference values in Table II.

material	type	RAMAN shift	phonon energy
Diamond	s	(1337.4 ± 0.2)	(165.83 ± 0.02)
Graphite	s	(1555.6 ± 0.2)	(192.89 ± 0.03)
Si	as	(517.3 ± 0.2)	(64.14 ± 0.02)
	s	(532.8 ± 0.2)	(66.07 ± 0.02)
CaF ₂	as	(323.5 ± 0.2)	(40.11 ± 0.02)
	s	(312.7 ± 0.2)	(38.77 ± 0.02)

Table IV. Calculated intensity ratios for all samples. s/as denotes the column holding the STOKES/anti-STOKES value for those spectra that contained a visible anti-STOKES component. The logarithmic column gives the real difference between the STOKES and RAYLEIGH component (that is, without the notch filter) if the optical density of 5-6 of the notch filter⁹ is subtracted.

material	s/as	STOKES/laser	log(STOKES/laser)
Diamond	–	0.44	-0.36
Graphite	–	0.03	-1.48
Si	4.24	0.09	-1.03
CaF ₂	2.72	0.08	-1.12

For silicon, we get a sample temperature of 250°C and for calcium fluoride the result is 183°C. These temperatures are resulting from the high laser power and the focusing objective both heating the samples. For the other samples, the temperature could not be calculated, as the anti-STOKES peak is missing.

III.D Semiconductor

For a semiconductor with a direct bandgap, the intensity of the RAMAN components in the scattered light depends on the density of states (DOS). If the the energy of the incident photon is below the bandgap, the intermediate state of the RAMAN process is virtual and the DOS around this energy is zero. Hence, we expect the intensity of the inelastic scattered light to be low. If the energy of the incident photons is equal or above the bandgap, the DOS is not zero anymore for the relevant energies. Due to HEISENBERG principle and the short

lifetime of the intermediate states, there are many states with matching energy. Therefore, the RAMAN intensity should be much higher than before. For example, the bandgap of silicon is 1.1 eV which is smaller than the energy of one laser photon, 2.3 eV. In case the DOS at the bandgap energy is very high, resonant effects are likely to occur. This affects the transition into and from the intermediate states, hence the first and the last step in the FEYNMAN diagram.⁹ If the energy of the scattered photon is equal to the bandgap energy, electrons of the semiconductor may absorb the radiation, as the RAMAN process is not limited to the topmost atomic layer.

In eqn. 12, Γ denotes the linewidth. As a short lifetime of the intermediate states means a high linewidth, Γ can be used to discuss the behaviour of the probability for the RAMAN process at different energies. In the normal case, the lifetime is short and the linewidth is high. Hence, the probability is small. For the resonant case, Γ is small as the lifetime is higher. Therefore, the probability increases for resonant energies.

IV Discussion

In this experiment, we optimized the setup in order to record a spectrum containing RAMAN peaks. After further adjustment, we measured a clean spectrum for the diamond sample. However, for the current setup, we were unable to detect any STOKES peaks for any of the other samples. Using the data from a different group, we could measure RAMAN peaks at or nearby the expected positions. All those positions were statistically identical or compatible. As for the RAMAN shifts, the difference to the reference values was quite high, possibly due to the high sensitivity of the calculations to small deviations. For diamond, even the shift is matching very well, although it is not statistically compatible. For the other spectra, the difference is much higher, hence it might not be solely explained by numerical issues. As we do not know the experimental setup used by that group, it is hard to dive further into the discussion of this deviation.

In total, the setup has proved to give accurate results. Additionally, the measurement itself was stable and reproducible. Finally, the setup could be used as a quite expensive thermometer. However, the sensitivity of the spectrometer seems to be quite low. Perhaps two chained spectrometers would help to address that issue.

¹ A. Anderson, *The Raman Effect* (Dekker, 1973).

² C. Kittl, *Einführung in die Festkörperphysik* (Oldenbourg, 2006).

³ G. Czocholl, *Theoretische Festkörperphysik* (Springer, 2008).

⁴ J. M. Ziman, *Principles of the Theory of Solids* (Cambridge University Press, 1972).

⁵ W. Demtröder, *Experimentalphysik 3* (Springer, 2010).

⁶ G. Burns, *Solid State Physics* (Academic Press, 1985).

⁷ W. Demtröder, *Laserspektroskopie* (Springer, 1993).

⁸ P. Yu and M. Cardona, *Fundamentals of Semiconductors* (Springer, 1999).

⁹ F. Berlin, *Lab Course Introduction on Raman Spectroscopy* (FU Berlin, 2009).